Hydrogen storage in salt caverns: Sizing, dynamic modeling and application for energy system analysis

Inga Beyers[1], Steffen Brundiers[1], Dirk Zapf[2], Clemens Lohr[1], Astrid Bensmann[1,*], Richard Hanke-Rauschenbach[1]

[1]Leibniz University Hannover, Institute of Electric Power Systems, Appelstraße 9A, 30167 Hannover, Germany
[2]Leibniz University Hannover, Institute for Geotechnical Engineering, Welfengarten 1A, 30167 Hannover, Germany

*Corresponding Author: astrid.bensmann@ifes.uni-hannover.de

ABSTRACT

Hydrogen is expected to play an important role in future decarbonized energy systems. Large-scale, economical storage of hydrogen gas can be achieved with artificial salt caverns created in natural underground salt rock deposits by the process of solution mining. Experience in operating natural gas caverns and compressed air caverns has shown that cavern thermodynamics, i.e., dynamic pressure and temperature evolution, play an essential role in operating behavior and dynamically influence discharge and charge limits and thus the market opportunities of such storages.

In this work, we contribute two aspects to the current discourse on hydrogen caverns. Firstly, we present a dynamic model for hydrogen salt cavern storage, which is adapted to the simulation demands of the salt cavern as a *storage component in energy systems*. We combine this with a sizing approach to parametrize cavern models from very few input parameters. The model is validated by comparison with a commercial simulation software, "Kavpool", and shows excellent agreement.

Secondly, we apply future dynamic load profiles generated from energy system transformation models to this cavern model. We distinguish between two application cases: Power-to-Gas (P2G) hydrogen caverns the provision of green hydrogen to industry and Power-to-Power (P2P) hydrogen caverns in a future climate-neutral Germany. We quantify the impact of this dynamic behavior for the respective application cases. The results indicate that the P2P application in future energy systems subjects the cavern to higher relative discharge loads and higher cavern throughput. It further results in larger temperature swings than the P2G application and can lead to inadmissible flow velocities in discharge operation close to the minimum operating pressure.

1 INTRODUCTION

As an energy carrier, green hydrogen is expected to play an important role in the decarbonization of hard-to-abate sectors in the global energy system. Examples of this are the chemical industry, where hydrogen is needed as a chemical feedstock or in processes such as hydrogenation/hydrocracking, the steel-making industry, long-duration energy storage or H_2-based fuels for shipping and aviation. For effective decarbonisation, this needs to be green hydrogen produced by fluctuating renewable energy. The fluctuating nature of green hydrogen production necessitates cheap storage at scale. Hydrogen can be stored cost-effectively in salt caverns, which are large artificial underground storages created via solution mining.

There are currently only six hydrogen caverns in operation worldwide, at four locations (Clemens Dome, Moss Bluff, Spindletop in the USA, and Teesside in the UK) (Małachowska et al., 2022). These

https://doi.org/10.52202/077185-0068

caverns store grey hydrogen for the chemical industry. Because of this limited experience, there has recently been a surge in interest in hydrogen cavern demonstration projects in continental Europe and internationally (Warnecke and Röhling, 2021). The demonstration projects are flanked by an increase in research activities on hydrogen caverns. Earlier work focused on assessing storage potential, with national scope (Fleig et al., 2020) or broader scope, e.g., Europe (Caglayan et al., 2020). There is currently a strong focus on technical aspects of hydrogen storage (for an overview see Réveillère et al., 2022), such as cavern tightness, cavern thermodynamics, hydrogen solubility with the sump (residual brine at the cavern bottom), interaction with microorganisms, adverse geochemical reactions and consequences of hydrogen for equipment. The first results indicate technical feasibility (Réveillère et al., 2022).

Newly built greenfield caverns can be designed and optimized for the requirements of future hydrogen storage. However, the transformation of existing natural gas caverns to hydrogen caverns, i.e., the hydrogen-readiness of existing caverns, is another active research question. First feasibility studies (Bültemeier et al., 2022) have focused on technical aspects but have not studied dynamic cavern operation beyond simple, exemplary load profiles. The consensus is that cavern operation in the future will be more flexible, i.e., more dynamic, with a higher number of cycles and more changes from charge to discharge and vice versa. So far, there have been no attempts to quantify the effects this will have on existing cavern infrastructure. Large-scale energy system transformation models can estimate load profiles for future caverns. In this paper, we combine these load profiles with a state-of-the-art, physically meaningful cavern model to quantify the impact of this increasingly dynamic and flexible operation. The problem lies at the intersection of thermodynamics, geomechanics, and energy systems and needs to harmonize those three disciplines to provide an answer.

This paper is structured as follows: Section 2 details the parametrization, sizing and modeling methodology. In Section 3, the two application cases are introduced. Section 4 presents and discusses the results. Section 5 summarises key findings and concludes the work.

2 METHODOLOGY

2.1 Cavern parametrization and sizing

An energy storage component is characterized by an energy capacity E and how quickly it can be charged/discharged, expressed by the power limits $P^{\max}_{\text{char}}$ and $P^{\max}_{\text{disch}}$. The energy capacity of a hydrogen cavern is dominated by the chemical energy of the hydrogen gas contained within. The inner thermal energy of the gas, determined by pressure and temperature, is negligible in comparison. Consequently, treating a salt cavern as a vessel only, the energy capacity is proportional to the mass of the hydrogen "working gas" and can be described with Equation (1):

$$E_{\text{LHV}} = m_{\text{wg}} \cdot \text{LHV}_{\text{H2}} \qquad E_{\text{LHV}} = V_{\text{wg,norm}} \cdot \rho_{\text{norm}} \cdot \text{LHV}_{\text{H2}} \tag{1}$$

Salt cavern specialists usually quantify cavern capacity with the norm-volume $V_{\text{wg,norm}}$ at $T = 273.15\,\text{K}$ and $p = 101,325\,\text{Pa}$ of the working gas. The term "working gas" is used in this context because a cavern is never discharged fully but rather operates between two pressure levels $p^{\max}_{\text{cav}}$ and $p^{\min}_{\text{cav}}$. These pressure levels are a function of the geostatic pressure p_{geo} of the cavern surrounding. The geostatic pressure is exerted by overlying rock layers (a sedimentary rock layer of the height H_{sedr} and a salt rock layer of the height H_{sr}) and gives a salt cavern its structural stability to contain high-pressure gas. An overview of the cavern structure and parameters is given in Figure 1. If H_{sedr} and H_{sr} are unknown, we suggest ratios of H_{sedr}:H_{sr} between 1:1 (shallow caverns) and 10:1 (deep caverns).

The critical structural point of a cavern is its roof because it is the point with the lowest geostatic pressure. The critical geostatic pressure p_{geo} at the cavern roof is thus:

$$p_{\text{geo}} = g \cdot \rho_{\text{sedr}} \cdot H_{\text{sedr}} + g \cdot \rho_{\text{sr}} \cdot H_{\text{sr}} \tag{2}$$

The geostatic pressure must always be higher than the maximum operating pressure plus a safety margin:

$$p^{\max}_{\text{cav}} = p_{\text{geo}} \cdot f^{\max}_{\text{p}}, \quad f^{\max}_{\text{p}} = [0.7, 0.9] \qquad p^{\min}_{\text{cav}} = p_{\text{geo}} \cdot f^{\min}_{\text{p}}, \quad f^{\min}_{\text{p}} = [0.2, 0.3] \tag{3}$$

https://doi.org/10.52202/077185-0068

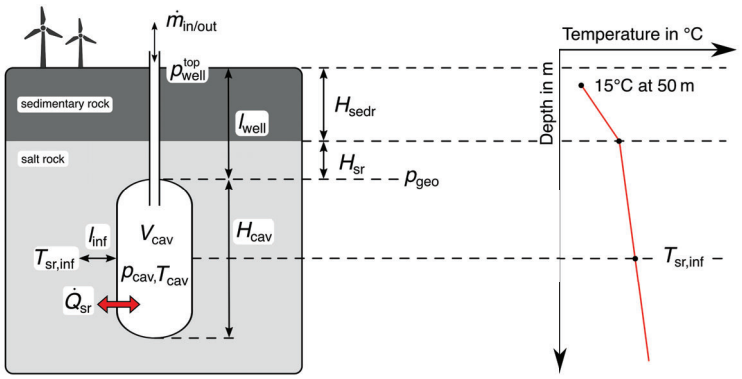

Figure 1: Overview of cavern model parameters, geometry and nomenclature.

The cavern gas densities can then be calculated with an estimate for the minimum and maximum cavern temperature, $T_{cav,est}^{min}$ and $T_{cav,est}^{max}$:

$$\rho_{cav}^{max} = \frac{p_{cav}^{max} \cdot M_{H2}}{z\left(p_{cav}^{max}, T_{cav,est}^{max}\right) \cdot R_m \cdot T_{cav,est}^{max}}, \qquad \rho_{cav}^{min} = \frac{p_{cav}^{min} \cdot M_{H2}}{z\left(p_{cav}^{min}, T_{cav,est}^{min}\right) \cdot R_m \cdot T_{cav,est}^{min}}, \tag{4}$$

with z being the compressibility factor of the working gas (real gas behaviour must be considered). With the minimum and maximum densities, the mass of the working gas is:

$$m_{wg} = (\rho_{cav}^{max} - \rho_{cav}^{min}) \cdot V_{cav} \tag{5}$$

The discharge power is limited by the permissible gas flow in the wellbore:

$$P_{disch,LHV}^{max} = \dot{m}^{max} \cdot LHV_{H2} \tag{6}$$

The existing cavern literature usually specifies a volumetric maximum withdrawal/injection rate in m^3/h at norm conditions. These limits originate from gas flow velocity limits v^{max}, so that the wellbore and equipment do not suffer from erosion (Bültemeier et al., 2022). The current limit used in natural gas caverns is $v^{max} = 20\,m/s$, but it is estimated that this could be increased up to $v^{max} = 25\,m/s$, because hydrogen gas flow is less erosive (Bültemeier et al., 2022).

$$\dot{m}^{max} = v^{max} \cdot \rho_{cav}^{min} \cdot A_{well} \tag{7}$$

2.2 Dynamic cavern model

Thermodynamic modeling of salt caverns has been undertaken at various levels of complexity, depending on the model's purpose. This work aims to capture the essential thermodynamics relevant to a cavern as a storage element within an energy system. The model thus needs to provide 1) the State-of-Energy (SOE), 2) thermodynamic state variables (pressure, temperature) to check the adherence to their respective limits, and 3) a translation of charge/discharge power to physically relevant quantities (e.g., the flow velocity), to check the adherence to limits as well. The model must provide all the elements listed above but still be simple enough that a time series analysis (e.g., hourly load profile of a year) is computationally feasible.

We define the SOE with the ratio of hydrogen masses:

$$SOE = \frac{m_{cav} - \left(m_{cav}^{max} - m_{wg}\right)}{m_{wg}} \tag{8}$$

https://doi.org/10.52202/077185-0068

The cavern pressure and temperature are governed by the cavern mass balance in Equation (9), and energy balance in Equation (10). For simplicity, we assume a uniform temperature and pressure within the cavern.

$$\frac{\mathrm{d}m_{\mathrm{cav}}}{\mathrm{d}t} = \dot{m}_{\mathrm{in}} - \dot{m}_{\mathrm{out}} \tag{9}$$

$$m_{\mathrm{cav}} \cdot \frac{\mathrm{d}u_{\mathrm{cav}}}{\mathrm{d}t} + u_{\mathrm{cav}} \cdot \frac{\mathrm{d}m_{\mathrm{cav}}}{\mathrm{d}t} = \dot{Q}_{\mathrm{cav,sr}} + \dot{m}_{\mathrm{in}} \cdot h_{\mathrm{in}} - \dot{m}_{\mathrm{out}} \cdot h_{\mathrm{out}} \tag{10}$$

The fluid properties are not explicitly included within the model formulation, but are accessed via the Coolprop fluid property library (Bell et al., 2014). Coolprop computes real gas properties with equations of state evaluated via Helmholtz energy formulations.

Heat is transferred between the cavern gas and the surrounding salt rock. The actual cavern surface is estimated with a factor $f_{\mathrm{V/A}} = V_{\mathrm{cav}}/A_{\mathrm{cav}}$, which can take the value range $f_{\mathrm{V/A}} = [8\,\mathrm{m}, 12\,\mathrm{m}]$ (Bérest, 2019). The heat transfer $\dot{Q}_{\mathrm{cav,sr}}$ via natural convection from the gas into the wall (and vice-versa) is calculated by:

$$\dot{Q}_{\mathrm{cav,sr}} = U \cdot A_{\mathrm{cav}} \cdot (T_{\mathrm{wa}} - T_{\mathrm{cav}}) \tag{11}$$

The heat transfer coefficient for convection at the cavern wall is critical to model fidelity. It typically lies in the range of $10 - 50\,\mathrm{W/m^2K}$ and constant heat transfer coefficients have shown unsatisfactory results (Raju and Kumar Khaitan, 2012). For hydrogen stored in salt caverns the relation proposed by Nieland (2008) has established itself:

$$U = 0.1 \left(\frac{\beta \cdot g \cdot \rho_{\mathrm{cav}}^2 \cdot |T_{\mathrm{wa}} - T_{\mathrm{cav}}| \cdot c_{\mathrm{p}} \cdot k^2}{\mu} \right)^{(1/3)} \tag{12}$$

The second heat transfer mechanism considered is non-stationary heat conduction within the surrounding salt rock. Nielsen and Leithner (2009) have proposed treating this as conduction in a semi-infinite cylinder with the Fourier differential heat conduction shown in Equation (13):

$$\frac{\partial T_i}{\partial t} = \alpha_{\mathrm{sr}} \left(\frac{\partial^2 T_i}{\partial r^2} + \frac{1}{r_i} \frac{\partial T_i}{\partial r} \right) \tag{13}$$

The temperature signal of the cavern can only penetrate a limited distance $l_{\mathrm{inf}} = \sqrt{k_{\mathrm{sr}} \cdot t_{\mathrm{inf}}}$ into the salt rock (Bérest, 2019). The temperature is assumed to be constant at this distance from the cavern wall. The temperature value $T_{\mathrm{sr,inf}}$ (see Figure 1) can be calculated with the geothermal gradients γ_{sedr} and γ_{sr} of the overlying rock layers:

$$T_{\mathrm{sr,inf}} = 15^{\circ}C + (H_{\mathrm{sedr}} - 50\mathrm{m}) \cdot \gamma_{\mathrm{sedr}} + (H_{\mathrm{sr}} + 0.5 \cdot H_{\mathrm{cav}}) \cdot \gamma_{\mathrm{sr}} \tag{14}$$

The temperature $T_{\mathrm{sr,inf}}$ is one boundary condition for the heat conduction equation; the other boundary condition is formulated with the wall termperature T_{wa}. For details regarding the discretization scheme and determination of T_{wa}, please refer to Nielsen and Leithner (2009).

The wellbore is modeled as an adiabatic, static pipe (neither mass nor energy storage within pipe) with a mass balance, momentum balance and energy balance between the welltop and wellbottom. In reality, the well flow velocity is different at every point in the well, but for simplicity, the pipe is considered as a single segment with the average well flow speed $\overline{v}_{\mathrm{well}} = 0.5 \cdot \left(v_{\mathrm{well}}^{\mathrm{top}} + v_{\mathrm{well}}^{\mathrm{bot}} \right)$. The hydrogen state at the wellbottom is equivalent to the cavern hydrogen state. The momentum balance is:

$$0 = A_{\mathrm{well}} \cdot \left(p_{\mathrm{cav}} - p_{\mathrm{well}}^{\mathrm{top}} \right) - A_{\mathrm{well}} \cdot d_{\mathrm{well}} \cdot g \cdot l_{\mathrm{well}} + \rho \cdot \frac{v_{\mathrm{well}}^{\mathrm{bot}} \cdot |v_{\mathrm{well}}^{\mathrm{bot}}|}{2 \cdot d_{\mathrm{well}}} \cdot \lambda_{\mathrm{well}} \cdot l_{\mathrm{well}} \tag{15}$$

The friction factor λ of the wellbore is calculated by the approximation of the Darcy-Colebrook equation for turbulent fluid flow ($Re \geq Re_{\mathrm{crit}}$) by Swamee and Jain, 1976.

https://doi.org/10.52202/077185-0068

2.3 Fundamental cavern behaviour

In this section, we show the fundamental thermodynamic behavior of the cavern model through an exemplary discharge-hold-charge sequence applied to a "reference cavern". Because salt caverns are bespoke components, no two caverns are the same. However, Bültemeier et al. (2022) have defined a reference cavern, which we use for the entirety of the remaining analysis. The reference cavern parameters are listed in Table 1, along with other model parameters. We calculate further missing parameters with the approach detailed in Section 2.1. The reference cavern behavior resulting from the discharge-hold-charge sequence is shown in Figure 2.

Table 1: Parameters of reference cavern (input parameters and other model parameters)

Parameter, from Bültemeier et al. (2022)	Value	Unit	Parameter, from Bérest (2019)	Value	Unit
Depth $H_{\mathrm{cav}}^{\mathrm{min}}$, $H_{\mathrm{cav}}^{\mathrm{max}}$	1100 – 1400	m	Shape factor $f_{\mathrm{V/A}}$	10	m
Geometric volume V_{cav}	500 000	m^3	Density ρ_{sedr}	2100	$\mathrm{kg/m}^3$
Maximum pressure $p_{\mathrm{cav}}^{\mathrm{max}}$	185	bar	Density ρ_{sr}	2160	$\mathrm{kg/m}^3$
Minimum pressure $p_{\mathrm{cav}}^{\mathrm{min}}$	60	bar	Thermal gradient γ_{sedr}	$3.2 \cdot 10^{-2}$	K/m
Wellbore diameter d_{well}	0.22	m	Thermal gradient γ_{sr}	$1.6 \cdot 10^{-2}$	K/m
Wellbore roughness	0.1	mm	Penetration length l_{inf}	10	m

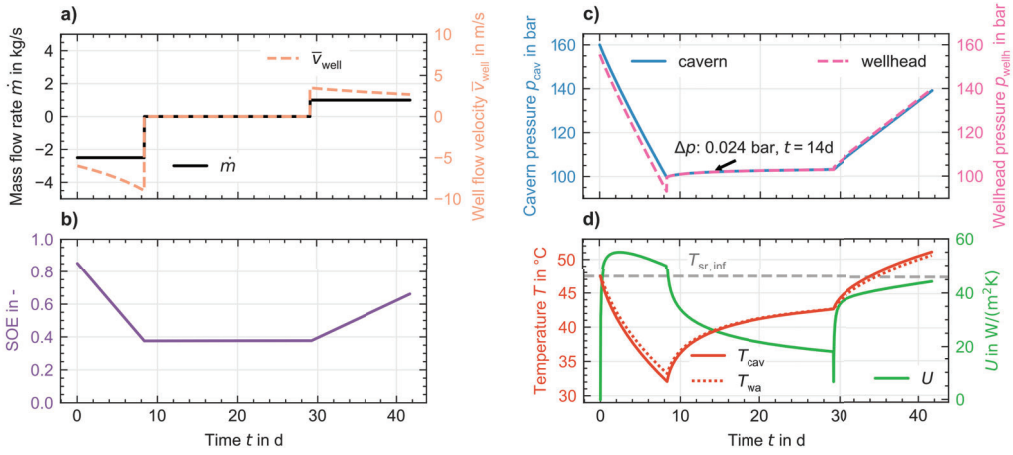

Figure 2: Fundamental cavern behaviour as visualized with an exemplary discharge-hold-charge sequence

Figure 2 a) shows the mass flow rate during the discharge phase (withdrawal, constant mass flow rate), followed by a holding phase, followed by a charge phase (injection, constant mass flow rate). Figure 2 b) visualizes the SOE over time. The SOE decreases linearly due to the constant $\dot{m}$ withdrawn, remains constant during the holding phase, and increases linearly during the constant $\dot{m}$ charge.

The cavern pressure, shown in Figure 2 c) largely mirrors the progression of the SOE variable but differs during the holding phase. In the holding phase, the heat transfer between the hydrogen gas and the surrounding cavern wall increases the gas temperature. Figure 2 d) shows the cavern gas temperature T_{cav} and wall temperature T_{wa} and the non-linear heat transfer coefficient U. The simulation is initialized from thermal equilibrium, which accounts for the relatively quick initial increase of U. The average flow velocity in the wellbore is plotted in Figure 2 a). It is important to note that the relationship between mass flow and the average well flow velocity is non-linear. In the discharge process, the pressure reduction causes a drop in hydrogen gas density. At a constant $\dot{m}$ withdrawal, this leads to an increased volume flow rate and thus increased flow velocity in the wellbore. Figure 2 c) additionally contains the pressure at

https://doi.org/10.52202/077185-0068

the wellhead, which differs from the cavern pressure. During discharge, the wellhead pressure is lower than cavern pressure, as pressure losses are incurred along the path from cavern to wellhead. Due to the increase in well flow speed, the pressure difference increases over time. In the holding phase, the Δp between wellhead pressure and cavern pressure is not discernible in the figure. However, a small Δp of 0.024 bar is due to the geodetic height difference between the cavern and the wellhead. During charging, the wellhead pressure must be larger than the cavern pressure to compensate for losses incurred along the wellbore.

We use the cavern pressure and temperature curve to validate the results with a commercial cavern simulation tool, "Kavpool". The results, found in the Appendix, shown an excellent argreement.

3 APPLICATION CASES

In the subsequent analysis, the reference cavern and model are subjected to hydrogen load profiles generated from energy system simulations. In this section, the origin of these profiles is briefly outlined.

Two different applications are analyzed for caverns in future energy systems: Firstly, as components in Power-to-Power (P2P) long-duration energy storage, and secondly, as Power-to-Gas (P2G) storage to provide hydrogen for industrial processes. We use data generated by the ESTRAM energy system transformation model (Lohr, Schlemminger, et al., 2022) for both applications. The P2P load profiles are taken from Lohr, Peterssen, et al. (2023), while the P2G profiles originate from Niepelt et al. (2023).

In the P2P case, the cavern load profiles result from a complete energy system model for a decarbonized Germany in 2045, that replicates the transformation pathway KN2045 outlined by Prognos et al. (2021). The model considers demands in all sectors, grid, storage, multiple sources, multiple energy carriers, and imports. The model is formulated as a linear optimization problem and optimized in an hourly resolution, with the objective of minimizing annual system costs. The simulation results are shown in Figure 3.

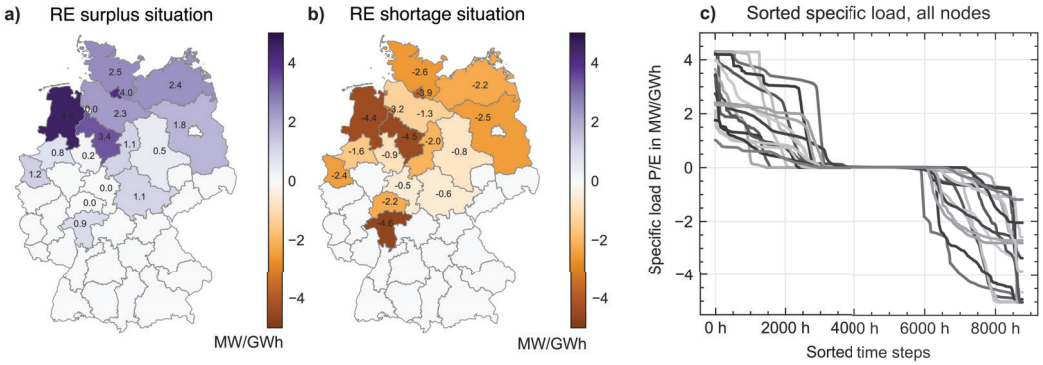

Figure 3: Visualization of the spatial resolution and specific loads for the P2P application case

To scale the load profiles to the cavern capacity, the load profiles are expressed as a specific load of power per storage capacity P/E. Figure 3 a) and b) show the specific load (in MW/GWh) in two arbitrarily chosen timesteps ($t = 10$ h with renewable energy surplus, $t = 1000$ h with renewable energy shortage). The timesteps show the spatial resolution of the model, which corresponds to the NUTS-2 level. These smallest geographical units are referred to as nodes in this work. As seen in both Figure 3 a) and b), not all nodes have hydrogen cavern loads because the geological potential for salt caverns is geographically constrained to middle and northern Germany. The 17 nodes with salt cavern potential result in 17 different load profiles. To provide some systematic insight into these load profiles, they are shown in Figure 3 c) sorted by magnitude from positive values (charge) to negative values (discharge). No limits are implemented for the specific load by the optimization model, as the assumption is that these are additional greenfield caverns that can be constructed to comply with the maximum P/E. The sorted

https://doi.org/10.52202/077185-0068

specific timesteps vary in magnitude and distribution, but generally, the timesteps have a split of 1/3 charge, 1/3 hold, and 1/3 discharge.

In the P2G case, Niepelt et al. (2023) formulated an industrial green hydrogen demand profile and optimized stand-alone systems to provide this green hydrogen in the year 2030. The hydrogen demand profile has little variation (200 kilotons p.a., 100 % load Mo-Fr 07:00-24:00, 80 % load Mo-Fr 00:00-07:00 and Sat-Sun 07:00-24:00, 60% load Sat-Sun 00:00-07:00, no seasonal variation). The study focuses on the impact of electrolyzer costs and assumes underground storage potential independent of location to show these effects better. Furthermore, all European NUTS-3 codes are analyzed, irrespective of whether the type of industry that requires hydrogen is present in the region. Therefore, we have selected 14 nodes in Germany for further analysis, where both salt cavern potential and industrial demand are present. An overview of the resulting load profiles is presented in Figure 4. Analogous to the P2P case, we show the two arbitrarily chosen timesteps in a) and b). The sorted timesteps in c) reveal three key differences: 1) no holding periods due to the constant hydrogen demand and the cavern's buffer storage function, 2) less variation between nodes, and 3) lower maximum specific loads in the discharge direction.

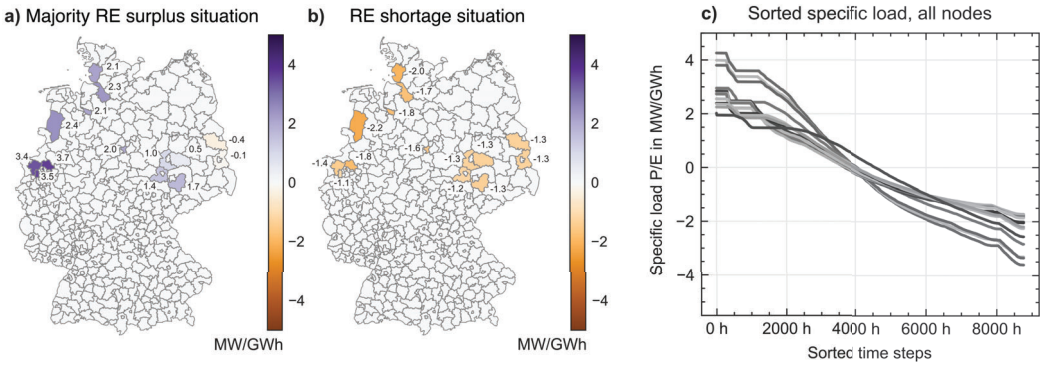

Figure 4: Visualization of the spatial resolution and specific loads for the P2G application case

4 RESULTS AND DISCUSSION

4.1 Selected cavern profiles

In this subsection, two complete year-long profiles of the relevant variables are shown and discussed in detail (one for P2P and one for P2G, respectively). Figure 5 shows the simulation results for the two cases. The choice of nodes is made arbitrarily. The profiles are, therefore, used to demonstrate certain effects and general tendencies but are not representative of all the nodes of their respective application.

Figure 5 a) contains the selected result for the P2P application and Figure 5 b) for the P2G application. The topmost graph shows the SOE over time. The SOE start and end values are identical, which is a constraint in the energy system transformation models from which the cavern load profiles originate. The P2P case has an overarching seasonality (charging predominantly in spring and summer, discharging predominantly in autumn and winter). However, it is not only seasonal storage but also utilized to balance the energy system. This balancing role can be quantified by calculating the number of equivalent cycles $n_{\mathrm{eq}} = \sum_{t=0}^{t=8760\mathrm{h}} \dot{m}_{\mathrm{out}}(t)/m_{\mathrm{wg}}$. In the P2P case, this results in $n_{\mathrm{eq}} = 6.08$. Allowing for some fluctuations, the n_{eq} values of purely seasonal storage would be in the range $n_{\mathrm{eq}} = [1, 2.5]$. In the P2G case, there is no discernible seasonality. Although the hydrogen supply by renewables is subject to seasonality, the relatively constant hydrogen demand profile behind the P2G simulation weakens the seasonality effect for this particular node. The cavern throughput lies in a similar range with $n_{\mathrm{eq}} = 5.69$.

The second graph from the top contains the pressure curve. In both cases, the pressure curve is almost identical to the SOE curve because there are no extended holding periods where thermal effects cause

https://doi.org/10.52202/077185-0068

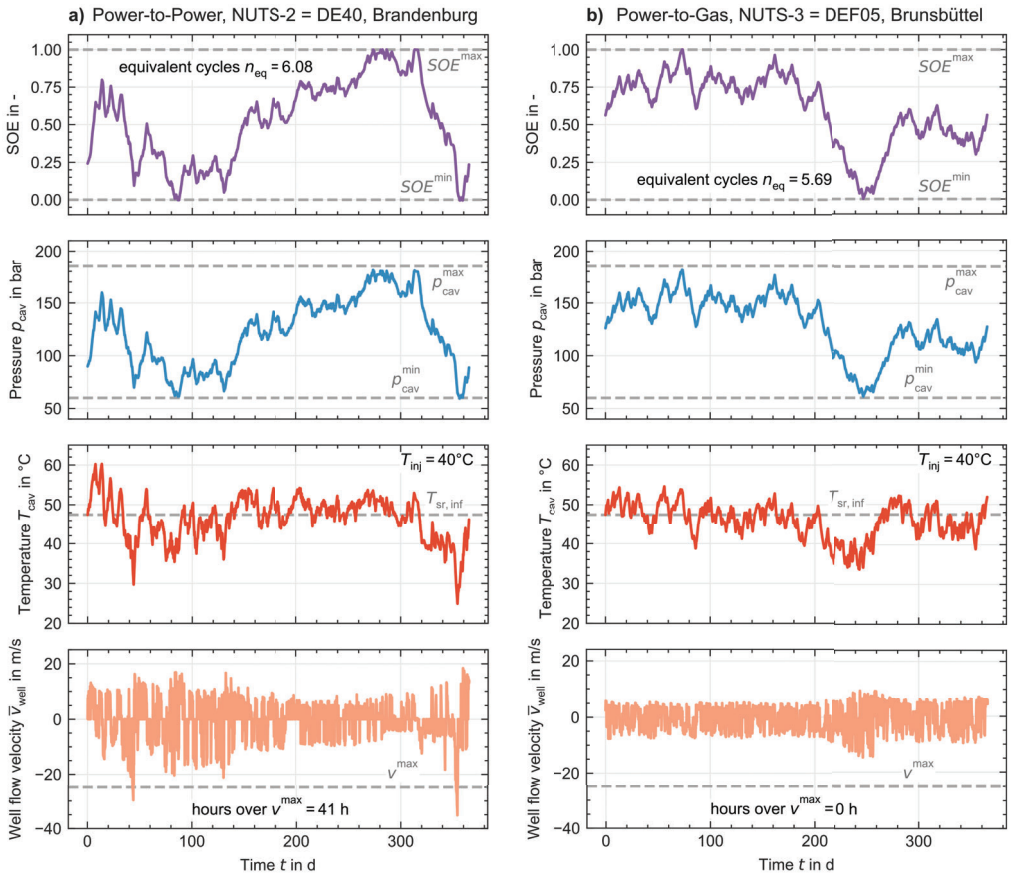

Figure 5: Key cavern variables over time for selected profiles

a noticeable divergence between SOE and pressure. The pressure stays within the pre-defined limits because the calculation of m_{wg} under consideration of $T_{cav,est}^{max}$, $T_{cav,est}^{min}$ allows for a sufficient margin.

The temperature curve (third from the top) fluctuates around $T_{sr,inf}$, with some significant temperature dips due to fast discharge at low pressures in the P2P case. Large ΔT values lead to a higher geomechanical stress on the salt cavern. In the P2G temperature curve, the ΔT between maximum and minimum temperature is not as large, which is consistent with the relatively constant hydrogen demand profile behind the simulation. It must be noted here that all simulations are initialized at $T_{cav}\ (t = 0) = T_{sr,inf}$. This start temperature is a simplification because caverns are continuously operating, and neither the hydrogen gas nor the first layers of saltrock will necessarily be in thermal equilibrium with the deeper saltrock layers. Experience has shown that, due to the large thermal inertia of salt caverns, the start temperature influences the cavern temperature in simulations for an extended period. This influence is not studied here but should be an aspect of further work.

The last diagram shows the flow velocity. In the P2P curve, the flow velocity exceeds $v^{max} = 25\,m/s$ for 40 hours. The crossing of v^{max} occurs when the cavern is discharged rapidly near p_{cav}^{min}. At low cavern pressures, the extracted gas has a lower density. The hydrogen discharged thus has a higher volume flow rate and, therefore, higher well flow velocities. No component management is implemented to prevent these high flow velocities in this simulation. The aim here is to demonstrate the effects and quantify the problem. Importantly, this does not mean that a) the load profiles from the energy system simulations are wrong or b) existing caverns cannot be repurposed for future hydrogen storage. The implication is that the optimal future cavern, sized as a greenfield cavern, has a different P/E ratio than the current standard

https://doi.org/10.52202/077185-0068

natural gas cavern. This mismatch is unsurprising because current caverns were built for seasonal natural gas storage rather than intra-day and intra-week balancing. In the P2G case, v^{max} is not exceeded.

4.2 Quantitative comparison of cavern loading

The analysis shown in Section 4.1 is repeated for all 17 P2P and 14 P2G nodes, resulting in many different time series. We aggregate the results of all nodes in Figure 6.Figure 6 a) shows the cavern throughputs n_{eq} for the P2P and P2G case respectively. In the P2P case, the distribution is bimodal, with one group between n_{eq} = 1.5 and n_{eq} = 3.7 (predominantly seasonal storage) and the other group between n_{eq} = 5.4 and n_{eq} = 11.4 (seasonal storage and balancing). In the P2G case, the caverns are all cycled strongly and the cavern throughput is similar, indicated with a smaller range of n_{eq} between 5.2 and 9.8.

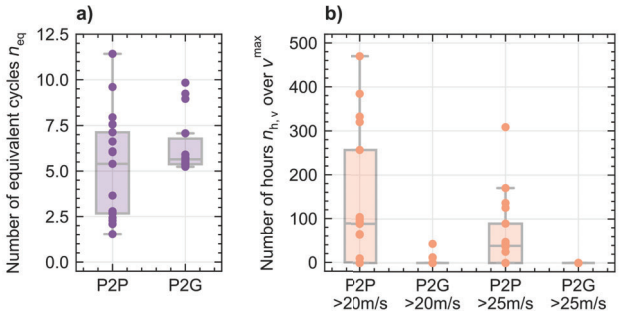

Figure 6: Aggregated node results to quantify the impact of dynamic operation

Figure 6 b) shows the number of hours that v^{max} is exceeded for every application. The number of hours was evaluated at two different limits: 20 m/s as the current flow velocity limit for natural gas caverns and 25 m/s as the current estimate of what could be acceptable, considering the reduced erosive effect of hydrogen flow. The 20 m/s limit is exceeded from 0 h to up to 470 h (which correspoonds to 5.4 % of time, annually). In the P2G case, only two nodes exceed 20 m/s and only for a few hours, and there is no exceedance of 25 m/s. The results thus indicate that the utilization profile of P2G applications can be considered unproblematic for existing caverns. In the P2P case, there are still crossings of 25 m/s of up to 309 h (which corresponds to 3.5 % of time, annually). This has several possible implications concerning existing caverns as future hydrogen storage. A positive aspect is that limit exceedance in the magnitude of 5 % of annual time is not much in relative terms. In those periods, adherence to flow limits would reduce some of the cavern throughput and thus forego some potential revenue, but not all. Another option is to qualify existing systems for higher flow velocities. Hydrogen is expected to have a less erosive effect than natural gas, and current standards for natural gas might not be directly applicable. This is currently an active area of research. An implication for the design of future caverns is to make provisions for dynamic operation and higher specific loads by planning larger wellhead diameters than currently typically found in caverns (0.2 – 0.3 m). However, wellboring is costly, and the decision is subject to economic benefits for the cavern owning/operating entity.

4.3 Variation of injection temperature

The previous analyses were conducted with a hydrogen injection temperature of T_{inj} = 40°C. There is currently no consensus on the injection temperature; values between 20°C – 40°C are proposed in the literature. The choice of injection temperature is a compromise between two opposing effects. High injection temperatures result in higher cavern temperatures, which increases salt rock creep. Salt rock is a viscous material, albeit with a very low viscosity. Higher cavern temperatures thus accelerate the natural capacity loss experienced by a salt cavern throughout its lifetime. Lower injection temperatures result in lower cavern temperatures but require a higher cooling effort before cavern injection.

https://doi.org/10.52202/077185-0068

Figure 7 shows the temperature distribution in the reference cavern for both application cases and all nodes but with a variation in injection temperature. In both cases, the general tendency is clear: increasing the injection temperature increases the minimum occurring temperature, the median temperature, and the maximum occurring temperature. However, because of thermal inertia and heat transfer with the surrounding salt rock, a 10°C increase in injection temperatures does not translate to a 10°C increase in cavern temperature. In both applications, the data show that a 10°C increase results in an approximately 1.5°C increase in the median cavern temperature.

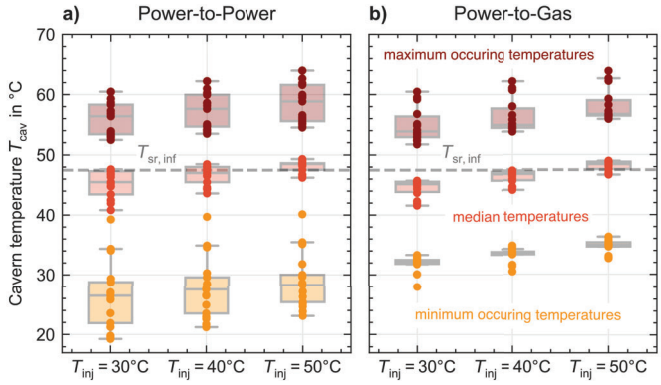

Figure 7: Impact of the variation of hydrogen injection temperature T_{inj}

A positive result is that the maximum occurring temperatures (64.0°C for P2P and 63.9°C for P2G at T_{inj} = 50°C) are significantly below safety-critical maximum temperatures (T = 80°C). The temperature variability is higher in the P2P application, which aligns with previous results. As mentioned previously, all simulations are initialized with $T_{sr,inf}$, and the impact of this has not been studied further.

5 CONCLUSIONS

This work presents a thermodynamic cavern model with an accompanying sizing strategy, which captures the relevant effects and limitations of hydrogen cavern operation as a storage component in future energy systems. The application of future load profiles to this cavern model delivers insights for both the cavern specialist perspective and the energy system modeling perspective, which are summarised here.

Cavern specialist perspective:

- The analyzed load profiles confirm an increasingly dynamic operation and higher cavern throughput of H_2 caverns in future energy systems.
- Current caverns, as represented by the reference cavern, are generally suited for future H_2 storage.
- High specific loads result in inadmissible flow velocities, but only up to 5 % of yearly time.
- The large temperature swings that result from this dynamic operation need to be input into more long-term geomechanical models to assess the effects on geomechanical stress.

Energy system modelling perspective:

- Charge and discharge limits are neither symmetric nor linear. The discharge process is generally more critical, and rapid discharge, close to P^{min}_{cav}, is especially critical.
- For large energy system models, where caverns are not represented with dedicated physical models, we propose $P^{max}_{char,LHV}/E_{LHV}$ = 4MW/GWh in the charge direction and $P^{max}_{disch,LHV}/E_{LHV}$ = 3 MW/GWh in the discharge direction as limits for existing caverns.

In further studies, the influence of the initial temperature should be studied. Furthermore, the results could be strengthened with additional load profiles since there are a number of different possible energy

https://doi.org/10.52202/077185-0068

system transition scenarios. Finally, this analysis should be repeated with different cavern configurations, as the influence of cavern parameters (size, shape factor, depth) has not been touched upon in this analysis.

NOMENCLATURE

Abbreviations

LHV	Lower heating value
MSA	Median symmetric accuracy
NUTS	Nomenclature of Territorial Units for Statistics
P2G	Power-to-Gas
P2P	Power-to-Power
RE	Renewable Energy
SOE	State-of-Energy

Latin Symbols

A	area
c	specific heat capacity
d	diameter
E	energy (capacity)
f	empirical factor
g	gravitational constant
h	specific enthalpy
H	height, depth
k	thermal conductivity
l	length
n	number of
$\dot{m}$	mass flow rate
m	mass
M	molar mass
p	pressure
P	power (capacity)
$\dot{Q}$	heat flow rate
r	radius
R	gas constant
Re	Reynolds-number
t	time
T	temperature
u	specific internal energy
U	heat transfer coefficient
v	velocity
V	volume
z	compressibility factor

Greek Symbols

α	thermal diffusivity
β	isobaric expansion coefficient
γ	geothermal temperature gradient
δ	difference
λ	friction factor
μ	dynamic viscosity
ρ	density

Superscripts and Subscripts

cav	cavern
char	charge
crit	critical
disch	discharge
eq	equivalent cycles
est	estimated value
geo	geostatic
H2	hydrogen
h,v	hours over maximum velocity
inf	infinite (cavern at rest)
inj	injection
m	molar
max	maximum
min	minimum
norm	norm conditions for gas
p	pressure
sedr	sedimentary rock
sr	salt rock
V/A	volume-area ratio
wa	wall
well	well
wellh	wellhead
wg	working gas

REFERENCES

Bell, I. H. et al. (2014). "Pure and Pseudo-pure Fluid Thermophysical Property Evaluation and the Open-Source Thermophysical Property Library CoolProp". In: *Industrial & Engineering Chemistry Research* 53.6, pp. 2498–2508. DOI: 10.1021/ie4033999.

Bérest, P. (2019). "Heat transfer in salt caverns". In: *International Journal of Rock Mechanics and Mining Sciences* 120, pp. 82–95. ISSN: 13651609. DOI: 10.1016/j.ijrmms.2019.06.009.

Bültemeier, H. et al. (2022). *Wasserstoff speichern - Soviel ist sicher*. Project Report. Bundesverband Erdgas, Erdöl und Geoenergie e.V. (BVEG).

Caglayan, D. G. et al. (2020). "Technical potential of salt caverns for hydrogen storage in Europe". In: *International Journal of Hydrogen Energy* 45.11, pp. 6793–6805. ISSN: 0360-3199. DOI: 10.1016/j.ijhydene.2019.12.161.

https://doi.org/10.52202/077185-0068

Fleig, S. et al. (2020). *InSpEE-DS- Information system salt structures: planning basis, selection criteria and estimation of the potential for the construction of salt caverns for the storage of renewables (hydrogen and compressed air)*. Project Report 03ET6062B. Federal Institute for Geosciences and Natural Resources (BGR).

Lohr, C., F. Peterssen, et al. (2023). *Integration of disamenity costs and equality regarding onshore wind power expansion and distribution into energy system optimization models*. DOI: 10.21203/rs.3.rs-3586294/v1.

Lohr, C., M. Schlemminger, et al. (2022). "Spatial concentration of renewables in energy system optimization models". In: *Renewable Energy* 198, pp. 144–154. ISSN: 0960-1481. DOI: https://doi.org/10.1016/j.renene.2022.07.144.

Małachowska, A. et al. (2022). "Hydrogen Storage in Geological Formations - The Potential of Salt Caverns". In: *Energies* 15.14, p. 5038. ISSN: 1996-1073. DOI: 10.3390/en15145038.

Nieland, J. D. (2008). "SALT CAVERN THERMODYNAMICS—COMPARISON BETWEEN HYDROGEN, NATURAL GAS, AND AIR STORAGE". In: *SMRI Fall 2008 Technical Conference*, pp. 1–19.

Nielsen, L. and R. Leithner (2009). "Dynamic Simulation of an Innovative Compressed Air Energy Storage Plant - Detailed Modelling of the Storage Cavern". In: *WSEAS TRANSACTIONS on POWER SYSTEMS*. Vol. 4.

Niepelt, R. et al. (2023). "The Influence of Falling Costs for Electrolyzers on the Location Factors for Green Hydrogen Production". In: *Solar RRL* 7.17, p. 2300317. ISSN: 2367-198X, 2367-198X. DOI: 10.1002/solr.202300317.

Prognos, Öko-Institut, and Wuppertal-Institut (2021). *Klimaneutrales Deutschland 2045 (Langfassung)*. Report 66-2021-DE. Stiftung Klimaneutralität, Agora Energiewende und Agora Verkehrswende.

Raju, M. and S. Kumar Khaitan (2012). "Modeling and simulation of compressed air storage in caverns: A case study of the Huntorf plant". In: *Applied Energy* 89.1, pp. 474–481. ISSN: 0306-2619. DOI: 10.1016/j.apenergy.2011.08.019.

Réveillère, A., C. Fournier, and M. Karimi-Jafari (2022). "Enabling Large-Scale Hydrogen Storage in Salt Caverns: Recent Developments". In: *SMRI Spring 2022 Technical Conference*, pp. 1–27.

Swamee, P. K. and A. K. Jain (1976). "Explicit Equations for Pipe-Flow Problems". In: *Journal of the Hydraulics Division* 102.5. Publisher: American Society of Civil Engineers, pp. 657–664. DOI: 10.1061/JYCEAJ.0004542.

Warnecke, M. and S. Röhling (2021). "Underground hydrogen storage – Status quo." In: *Journal of Applied and Regional Geology* 172.4, pp. 641–659. ISSN: 1860-1804. DOI: 10.1127/zdgg/2021/0295.

ACKNOWLEDGEMENTS

We thank Sebastian Günther for helpful discussions on time series features and Raphael Niepelt for providing his data of the P2G application case.

APPENDIX

The complete source code and all data used for this analysis are available in the following repository: https://github.com/ibeyers/ECOS_24_Analysis.git

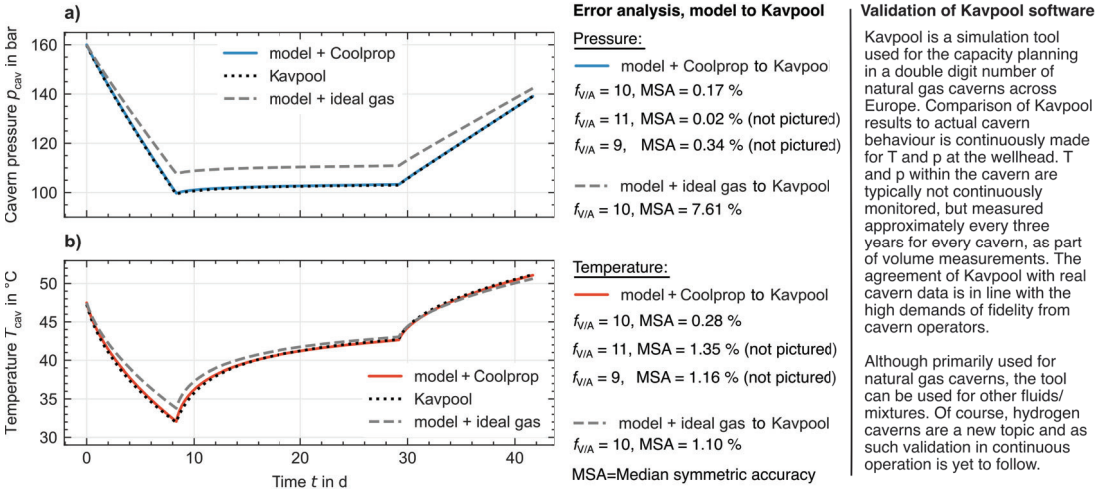

Figure A.1: Validation of a) pressure curve and b) temperature curve.

https://doi.org/10.52202/077185-0068